Perovskite (Sr2Ta2O7)100–x(La2Ti2O7)x ceramics: From dielectric characterization to dielectric resonator antenna applications

Mohamad Haydoura, Ratiba Benzerga, Claire Le Paven, Laurent Le Gendre, Vincent Laur, Alexis Chevalier, A. Sharaiha, Franck Tessier, François Cheviré

Perovskite $(Sr_2Ta_2O_7)_{100-x}(La_2Ti_2O_7)_x$ ceramics: from dielectric characterization to dielectric resonator antenna applications

M. Haydoura[1], R. Benzerga[1*], C. Le Paven[1], L. Le Gendre[1], V. Laur[2], A. Chevalier[2], A. Sharaiha[1], F. Tessier[3], F.Cheviré[3]

[1] Univ Rennes, CNRS, IETR UMR 6164, F-35042 Rennes, France.

[2] Univ Bretagne Occidentale, CNRS, LABSTICC UMR 6285, F-29 200 Brest, France.

[3] Univ Rennes, CNRS, ISCR UMR 6226, F-35042 Rennes, France

*Corresponding author: ratiba.benzerga@univ-rennes1.fr

Abstract

In this paper, ferroelectric ceramics with $(Sr_2Ta_2O_7)_{100-x}(La_2Ti_2O_7)_x$ (STLTO) compositions have been investigated and their dielectric properties have been characterized in wide frequency band (from few kHz to few GHz); their integration in Dielectric Resonator Antennas (DRA) was conducted. The dense STLTO ceramics have been obtained by high temperature sintering of powders synthetized by solid state chemistry route. STLTO crystalline cell parameters and volume vary linearly as a function of the chemical composition (x) thus demonstrating an ideal solid solution domain for $0 \leq x \leq 3$. Dielectric characterizations highlight that the permittivity and the dielectric loss vary according to the composition (x) and that the lowest losses are obtained for $x < 1.65$ compositions. The latter corresponds to the transition between the ferroelectric and paraelectric compositions of the STLTO material at room temperature. A low profile DRA structure was realized using a cylindrical paraelectric STLTO resonator (with x = 0) with a permittivity of 83 and losses $\tan\delta = 5 \times 10^{-3}$ @ 3.3 GHz. The DRA prototype was simulated,

produced and tested. It exhibits a hybrid $HEM_{11\delta}$ mode, with a resonant frequency at 5.80 GHz, a 4.9 % bandwidth and a gain of 6.4 dB. These features confirm the potential of the paraelectric STLTO compositions in compact antennas radiating at frequencies below 6 GHz.

***Keywords**: Perovskite Materials; Ceramics; Dielectric properties; Dielectric Resonator Antenna*

1. Introduction

With the development of modern communication devices, a small and high gain antenna becomes a requirement. One of the proposed solutions is the use of dielectric resonators as radiating elements, thus producing dielectric resonator antennas (DRA), offering good performance and providing an alternative solution to microstrip technology in terms of bandwidth, compactness and radiation efficiency due the absence of metallic loss [1,2]. The dielectric resonator can be manufactured in different geometrical shapes (cylindrical [3], rectangular [4], triangular [5], half-split cylindrical [6]...) and excited through the use of appropriate devices including coaxial probes [7], microstrip lines [8-9] or slots [10]. The DRAs thus produced, integrating low loss dielectric materials, have high efficiencies (> 85 %) [2, 11-12] and can operate at different frequencies, the latter being inversely proportional to the size of the dielectric resonator and to the permittivity of the dielectric material [3].

Conventional dielectric materials with low permittivity ($\varepsilon' < 20$) and very low loss ($\tan\delta < 10^{-3}$) were initially used for performing DRAs operating at microwaves frequencies, such as $Zn_3Nb_2O_8$ [13], $ZnMgTiO_3$ [14] or commercial dielectric materials, for example: ECCOSTOCK HiK [15] or Rogers RO3010 [16]. Other materials with higher permittivity values ($\varepsilon' > 20$), as $Ba_2Ti_9O_{20}$ [17] or $Ca_5Nb_2TiO_{12}$ [18], have been used in order to decrease the operating frequencies of the DRAs (typically < 6 GHz). Recently, the need for miniaturization and reduction of the operating

frequency has encouraged the use of materials with higher permittivity ($\varepsilon' \geq 60$) and losses typically around ($\tan\delta \approx 10^{-2}$ - 10^{-3}) in order to preserve an acceptable DRA gain and efficiency. This concerns ferroelectric materials such as $Ba(Ti_{1-x}Fe_x)O_{3-x/2}$ [19], $Sr(Zr_xTi_{1-x})O_3$ [20] or ferroelectric composite materials such as $Y_3Fe_5O_{12}/CaTiO_3$ [21] and $CaTiO_3$-$BiVO_4$ [22]. Perovskites or TTB (tetragonal tungsten bronze) dielectrics are also of interest, such as $CaTiO_3$ [23] and $Ba_4Nd_{9.3}Ti_{18}O_{54}$ (BNT) [24] respectively.

In this work, a new paraelectric/ferroelectric STLTO material is developed based on the combination of two ferroelectric perovskite compounds, i.e. $Sr_2Ta_2O_7$ and $La_2Ti_2O_7$, having Curie temperatures (T_C) of -107 °C and 1461 °C respectively. Previous work by Nanamatsu *and al.* [25] on the $(Sr_2Ta_2O_7)_{100-x}(La_2Ti_2O_7)_x$ solid solution in the form of single crystals and ceramics has shown that the T_C of these compounds can be tuned by adjusting their chemical composition (x). Our recent work [26] focused on the STLTO system with $0 \leq x \leq 5$ and included a full dielectric and ferroelectric characterization achieved in the kHz frequency range. In particular, Polarization-Electric field (P-E) measurements and characterization of the permittivity as a function of the temperature demonstrated the ferroelectric behavior of the STLTO ceramics with $x \geq 1.65$ compositions at room temperature, and so, the paraelectric behavior of the ceramics with $x \leq 1.5$.

The advantage of the STLTO compositions with x between 0 and 3 is the ability to select, at room temperature, the ferroelectric or paraelectric compositions according to the targeted application. For example, ferroelectric phases can be privileged for their agility, while paraelectric phases will be preferred for their moderate permittivities and low losses. The aim of the present study is to complete the dielectric characterization of the STLTO ceramics in the GHz range and to show the potential of the paraelectric STLTO compositions (here with $x = 0$) for

antenna applications. Our purpose is to present a study from the bench to the demonstrator, i.e., a dielectric resonator antenna based on the synthesized material.

The paper focuses first on the synthesis of different STLTO powders with composition (x) ranging from 0 to 3; then the manufacture of dense ceramics and their structural and morphological characterization are discussed. Next, we present the dielectric characterization of the STLTO ceramics in a wide frequency range, from a few kHz to a few GHz. Simulations, realization and measurement of a DRA based on the $x = 0$ paraelectric STLTO material (i.e. $Sr_2Ta_2O_7$) are finally exposed.

2. Materials and methods

2.1 STLTO material synthesis and characterization

In this study, different $(Sr_2Ta_2O_7)_{100-x}(La_2Ti_2O_7)_x$ compositions have been developed with $0 \leq x \leq 3$. The powders were first obtained by solid state chemistry route from stoichiometric mixture of carbonate and oxide precursors, i.e. $SrCO_3$, Ta_2O_5, La_2O_3 and TiO_2. The precursors were manually wet ground in isopropanol for 30 min using an agate mortar and then dried at 80 °C in an oven. The as-prepared mixtures were formed into pellets under a pressure of 70 MPa in order to improve reactivity during the heat treatment under air. The latter was carried out in two steps. First, the samples were calcined at 1000 °C for 15 h in a muffle furnace in order to decarbonate the strontium precursor and precombined the different elements. The samples were then ground and repelletized as above and finally heated at 1400 °C for another 15 h. STLTO ceramics were then manufactured by adding to the synthesized powders 5 %wt. of Rhodoviol, which is a low molecular weight polyvinyl alcohol (PVA) used as an organic binder. The obtained mixtures were pelletized at 230 MPa using a uniaxial press. The pellets

were heated under air, with a first step at 650 °C for 3 h in order to decompose and remove the PVA binder, and followed by a second step at 1500 °C (1400 °C for composition $x = 0$) for 2 h in order to densify the pellets.

X-ray diffractograms of the STLTO powdered samples were obtained at room temperature with a Panalytical X'pert Pro diffractometer (Cu K-$L_{2,3}$ radiation made of the K-L_2 line (λ = 1.54439 Å) and the K-L_3 line (λ = 1.54059 Å) with a ratio K-L_3 / K-L_2 = 0.5). Samples were analyzed through a θ–2θ scan with the 2θ angle ranging from 5° to 90°; scanning rate was 0.75°/min.

Surface morphologies and grain size of sintered STLTO ceramics were characterized using a scanning electron microscope (SEM JEOL JSM IT-100) operating at 20 kV.

2.2 Low frequency dielectric characterization techniques

For the low frequency dielectric characterization, i.e. in the kHz-MHz range, a Metal/Insulator/Metal structure (MIM) was used to determine the real part of the permittivity (relative permittivity ε', hereafter named as "permittivity") and the dielectric loss of the ceramic materials. The top and bottom surfaces of the STLTO ceramic samples, which are 13 mm in diameter and a few hundred of microns in thickness, were polished and then metallized by a 300 nm thick silver layer deposited by radio-frequency sputtering via a rigid mask.

The capacitance measurements at 10 kHz and 2 MHz were performed using an LCR meter (LCR-819 GWInstek) and a vector network analyzer (VNA) (Keysight E5061B ENA LF-RF VNA) respectively. The dielectric loss (tanδ) of the STLTO materials are directly given by the LCR meter and the VNA, while the permittivity (ε') values are calculated using the formula (1):

$$\varepsilon' = \frac{C \times t}{\varepsilon_0 \times A} \qquad (1)$$

where C = capacitance of the MIM structure (F), t = thickness of the ceramic (m), A = surface of the upper electrode (m^2) and ε_0 = permittivity of the vacuum (8.854×10^{-12} $F.m^{-1}$).

2.3 UHF band dielectric characterization techniques

For the characterization in the ultra-high frequency (UHF) band, STLTO ceramic pellets with a 16 mm diameter and a 3 mm thickness were used for both dielectric coaxial probe and dielectric resonant cavity analyses.

For the first one [27-28], dielectric characterization was performed using an Agilent N1501A dielectric probe connected to an Agilent vector network analyzer (Agilent E8364A); the Short-Open-Load (SOL) calibration was applied using the VNA calibration kit. This measurement technique gives direct access to the real (ε') and imaginary (ε") parts of the permittivity and thus to the dielectric loss (tanδ = ε"/ ε') of the STLTO ceramics in a frequency range from 1 to 20 GHz. Surfaces of the ceramics were polished in order to improve contact between the probe and the pellet surface.

For the second technique, measurements were done in the frequency range 0.5 – 15 GHz using a dielectric resonant $TE_{01\delta}$ cavity (QWED) connected to an Anritsu MS444B vector network analyzer. The real part of the permittivity is determined from the transmission parameter S_{21} signal by the shift of the resonance frequency peak as described in [29-31]; dielectric loss are then determined from the width at -3 dB of the shifted resonance peak. Dielectric properties are further calculated using the commercial cavity analysis software. The unloaded resonant cavity resonates at 14.5 GHz while the cavity loaded with the synthesized STLTO ceramics resonates in

the frequency range 1.98 – 3.32 GHz depending on the dimensions and permittivity value of the measured samples.

2.4 DRA prototype simulation and measurement techniques

The design and the simulation of the reflection coefficient (S_{11}) of the cylindrical dielectric resonator antenna structure (Figure 1) were done using the CST Microwave Studio software via the time domain solver. The dielectric resonator is placed on a RT5880 dielectric substrate and is excited directly by a 50 Ω open end microstrip line printed on the substrate. The overlap distance (D), between the center of the resonator and the open end of the microstrip line, determines the coupling strength, the specific mode that is excited, as well as the bandwidth of the antenna. The strongest coupling occurs when the overlap is slightly shorter than one-quarter of a microstrip guided wavelength at the resonance frequency. The dimensions of the microstrip line were obtained from a parametric simulation study assuming the best impedance matching.

The mode of operation and resonant frequency of the dielectric resonator (DR) with perfect magnetic walls can be calculated using the relations found in [3]. The resonant mode was later cross verified with the simulated E-H field distributions inside the DRA.

Measurement of the reflection parameter (S_{11}) of the DRA was performed using an Anritsu (MS444B) VNA. SOL calibration of the VNA was carried out using the Anritsu calibrating kit prior to measurements. Gain radiation patterns of the prototype were measured by the near field process measurements around the resonance frequency [35]. The main and crossed components in the E plane and the H plane have also been measured by varying the elevation angle θ and azimuthal angle ϕ all around the antenna from 0° to 360°.

3. Results and discussion

3.1 STLTO materials

The synthesized STLTO powders were analyzed by X-ray diffraction for phase identification. All patterns (see Supplementary File 1) were indexed as single phases isostructural with $Sr_2Ta_2O_7$ (orthorhombic, JCPDS-72-0921); no secondary phase is detected. As shown in Figure 2, the linear evolution of the relative variation of the a, b and c parameters and volume of the crystal lattice demonstrates the formation of an ideal $(Sr_2Ta_2O_7)_{100-x}(La_2Ti_2O_7)_x$ solid solution domain in the studied composition range ($0 \leq x \leq 3$).

The SEM surface microstructures of the STLTO ceramics, as shown in reference [26], allow to draw the evolution of the grain size of the STLTO ceramics as a function of the chemical composition (x) (Figure 3): the grain sizes are similar in between 2 and 4 μm with an average size of ~ 3 μm. Let us note that the $Sr_2Ta_2O_7$ (x = 0) composition pellet was sintered at a lower temperature (1400 °C) in order to obtain an average grain size close to 3 μm as the other compositions. Close attention has been paid to this aspect because, as Zhang *et al.* [36-37] pointed out on $Ba_{1-x}Sr_xTiO_3$ ceramics that it is crucial to control the grain size of ceramics which is a parameter greatly influencing their dielectric and ferroelectric properties. Furthermore, the grain size evolution show that a small addition of $La_2Ti_2O_7$ allows a more homogeneous growth of the grains in the $(Sr_2Ta_2O_7)_{100-x}(La_2Ti_2O_7)_x$ ceramics.

3.2 Low frequency dielectric characterization of STLTO materials

Figure 4 presents the evolution of the permittivity (ε') and the dielectric loss (tanδ) at 10 kHz and room temperature (RT) as a function of the composition (x) for $(Sr_2Ta_2O_7)_{100-}$

$_x(La_2Ti_2O_7)_x$ ceramics with $0 \leq x \leq 3$. One clearly observes that permittivity and losses vary with the composition, with a maximum of the permittivity ($\varepsilon' = 375$) obtained for the $x = 1.65$ composition. It is also worth noting that dielectric loss increase for $x \geq 1.65$ compositions in agreement with our previous P-E measurements emphasizing a ferroelectric behavior of the STLTO ceramics for $La_2Ti_2O_7$-rich compositions [26].

The evolution of the permittivity and dielectric loss at 2 MHz and RT as a function of the composition (x) of STLTO ceramics is presented in Figure 5. Measurements show an evolution fairly close to that obtained at 10 kHz, highlighting the dependence of ε' and $\tan\delta$ on the composition (x). Maximum permittivity values are obtained for compositions in the range $1.5 \leq x \leq 2$, with a maximum value $\varepsilon' = 280$ for $x = 2$. Very low dielectric loss values are detected for the $x \leq 1.5$ compositions; in fact, at such frequency, i.e. 2 MHz, some of the measured values are under the detection limit of the equipment (1×10^{-4}) and were therefore given equal to this value.

To our knowledge, no permittivity data on the STLTO compounds are available in the literature other than those reported in our previous study [26]. Concerning the $Sr_2Ta_2O_7$ end-member ($x = 0$), our value ($\varepsilon' = 88$) at 2 MHz is very close to the value $\varepsilon' \sim 85$ obtained at 0.25 MHz on $Sr_2Ta_2O_7$ ceramics by Hushur *et al.* [38]. On a similar layered $Sr_2Nb_2O_7$ perovskite, permittivity and dielectric loss were shown to be relatively unaffected up to a frequency of 5 MHz [39], with values around 48 for the permittivity and 4.2×10^{-3} for dielectric loss determined using MIM structures.

3.3 UHF dielectric characterization of STLTO materials

Results of the measurements using a coaxial probe are presented in Figure 6 with the evolution of the permittivity and dielectric loss at 2 GHz and RT as a function of the composition (x) of the STLTO ceramics. The graph shows a very similar variation to those obtained at 10 kHz and at 2 MHz with a maximum of the permittivity ($\varepsilon' = 190$) obtained for $x = 2$. The dielectric loss measured here are high compared to those obtained at 10 kHz and 2 MHz, especially for $x > 1.5$ with values as high as $\tan\delta = 0.2$.

Permittivity and dielectric loss resulting from measurements in the dielectric resonant cavity are presented in Figure 7. The quality factor, permittivity, dielectric loss values as well as the frequency of the measurement are summarized in Table 1. Once again, results emphasize the dependence of ε' and $\tan\delta$ with the composition (x), with a maximum permittivity value ($\varepsilon' = 231$) for $x = 2.0$ and losses decreasing down to few 10^{-3} for $x \leq 1.5$. These values are of the order of those measured by the coaxial probe technique, suggesting that the dielectric loss of the ferroelectric STLTO materials are higher in the GHz range than in the kHz and MHz ranges. Moreover, the permittivity values obtained by the resonant cavity method are somewhat higher than with the coaxial probe technique. This could be explained by the contribution of undesired air gaps between the probe and the sample surface, thus inducing an underestimation of the permittivity of the material under test in the case of the coaxial probe measurements. To our knowledge, no dielectric measurements have been operated on STLTO material or even $Sr_2Ta_2O_7$ or analogous ceramics in the GHz range, and so, comparison of our results to reported values cannot be made.

3.4 Integration of a STLTO ceramic in a dielectric resonator antenna

Based on the measurement results in the UHF frequency range, showing very low losses for $x \leq 1.5$ STLTO compositions, these new materials were tested in antenna applications, namely dielectric resonator antenna. Here are reported the first results relatively to the STLTO material with $x = 0$, that is the $Sr_2Ta_2O_7$ compound. This one presents the best compromise between low dielectric loss ($\tan\delta = 5 \times 10^{-3}$) and moderate permittivity ($\varepsilon' = 83$); these features are suitable for low profile DRA structures as reported in [4-11].

For the electromagnetic simulations of the antenna structure, dimensions of the microstrip feed line and positioning of the resonator on it were varied to achieve an impedance matching around 50 Ω and a resonant frequency between 5.5 and 6 GHz. The final proposed DRA geometry is presented in Figure 8. It consists of a cylindrical dielectric $Sr_2Ta_2O_7$ resonator with a radius (r) = 7.95 mm and a height (h) = 2.32 mm. It is excited by a copper microstrip line with a length (L_f) = 20 mm, a width (W_f) = 3.5 mm and a thickness of 17 µm. The copper feed line is printed on a rectangular RT5880 dielectric substrate ($\varepsilon' = 2.2$, $\tan\delta \sim 10^{-4}$) with 37 x 30 x 0.8 mm^3 dimensions. The back surface of the RT5880 substrate is covered by a 17 µm thick copper layer, which constitutes the ground plane. For the simulated and realized DRA prototype, it must be noticed that the discrete port is modeled by a lumped element, consisting of a current source with 50 Ω input impedance. The distance (D) between the end of the microstrip line and the center of the resonator, which affects the excited mode and the impedance matching of the antenna structure, was optimized and the final value is D = 1.2 mm. It is worth noting that, with this geometry, a compact antenna is obtained, having small radius compared to the wavelength with $ka < 1$ (a = radius of a sphere circumscribing the antenna and $k = 2\pi/\lambda$) [40]. The prototype of the

$Sr_2Ta_2O_7$ dielectric resonator antenna (Figure 8(b)) was further manufactured based on these parameters values.

Figure 9 shows the evolution of the simulated and measured reflection coefficient (S_{11}); a very good agreement between measurements and simulation is observed. Examining the simulated E-H field distributions at 5.80 GHz (Figure 10) and comparing them to theoretical ones [41], we can easily identify the hybrid $HEM_{11\delta}$ mode as the resonant mode of the simulated antenna. Experimentally, a minimum of the reflection loss is observed at the frequency of 5.80 GHz. It gives a bandwidth ($S_{11} \leq$ -10 dB) of 4.9 % between 5.65 and 5.95 GHz.

The far-field radiation patterns were measured in E and H planes over a 5.7 to 5.9 GHz frequency range with a 50 MHz step. Measurements for 5.80 GHz are shown in Figure 11 and for 5.7 GHz and 5.9 GHz in Supplementary File 2. One can first notice that all the patterns present a wide bandwidth with an almost constant gain and low cross polarization in the two planes. The radiation patterns remain stable with frequency and the measured patterns are similar to the simulated ones. The measured DRA exhibits a gain of 6.4 dB, around the central frequency, associated with an 80 % efficiency, equivalent to the simulated gain of the DRA obtained using CST Microwave Studio.

The attained results can be compared with similar DRA structures of the literature made with dielectric resonators having permittivity values ($82 < \varepsilon' < 97$) close to the selected $Sr_2Ta_2O_7$ ceramic ($\varepsilon' = 83$) and having similar shape (cylindrical) or being excited with the same excitation technique; characteristics of the measured reported DRAs [20,42-45] are summarized in Table 2. The later shows that our results are similar to that of literature. Moreover, it points out that our DRA presents a very good trade-off between dimensions, operating frequency, gain and

bandwidth. The present cylindrical dielectric resonator antenna offers a good impedance matching associated to a bandwidth of 290 MHz that is suitable for many practical applications using low profile antennas for short range wireless communications.

Concerning the material, STLTO cannot offer optimum characteristics as those of pure dielectrics [24] tailored to attain stable characteristics, because STLTO is a ferroelectric. In particular, a temperature coefficient (τ_f) of the resonant frequency equal to 480 ppm/° was measured around 3.6 GHz for the $Sr_2Ta_2O_7$ pellet, i.e. the x = 0 term of the STLTO solid solution. This value can be considered as relatively low considering the ferroelectric nature of the STLTO compounds and the intrinsic variation of their permittivity with temperature. This thermal drift will affect slightly the operation of the antenna, as predicted by our simulations which show a resonance frequency shift of only 1.4 % when passing from 20°C to 70°C. Moreover, pure dielectrics, such as the TTB $Ba_4Nd_{9.3}Ti_{18}O_{54}$ [24], present quality factors Qxf of 10 000 GHz with permittivities similar to ours, whereas $Sr_2Ta_2O_7$ offers a Qxf factor of 660 GHz. However the latter is close to that of the ferroelectric $Sr(Zr_xTi_{1-x})O_3$ material integrated in a DRA [20] such as the present one (see Table 2). Besides, some authors (S. Keyrouz *et al.* [34], Sebastian *et al.* [46], for instance) underline that quality factors in the range of 20 to 2000 are suitable for DRA. All this underlines that the paraelectric STLTO compositions, presenting moderate permittivities and low losses, are potentially good candidates for compact low profile DRAs.

4. Conclusions

In this work, an experimental investigation of the microwave dielectric properties of new ceramics is presented, followed by their integration into miniature dielectric resonator antennas.

The studied paraelectric/ferroelectric $(Sr_2Ta_2O_7)_{100-x}(La_2Ti_2O_7)_x$ (STLTO) compounds were obtained through chemical synthesis and sintering using solid-state procedures. The dielectric characterizations highlight a very similar evolution of the permittivity and the dielectric loss as a function of the composition (x) whatever the frequency range is. At 10 kHz, 2 MHz and 2 GHz, the maximum permittivity is obtained for the compositions (x) between 1.5 and 2. These results, correlated with dielectric loss which increase for the $x > 1.5$ compositions, confirms that the STLTO ceramics are in their ferroelectric state at room temperature for these compositions, and that for $x \leq 1.5$, they are in their paraelectric state with very low tanδ values in the order of a few 10^{-3}. Integrating a STLTO resonator with such low losses in a DRA is then of interest. This was done experimentally and numerically, taking advantage also of the moderate permittivity of these ceramics at few GHz. A first prototype of a DRA based on the STLTO (x = 0) ceramic with permittivity $\varepsilon' = 83$ and $\tan\delta = 5 \times 10^{-3}$ was produced and measured. The antenna consists of a cylindrical pellet of the $Sr_2Ta_2O_7$ material placed above a printed microstrip line which excites the hybrid $HEM_{11\delta}$ mode. The measured results are in very good accordance with the simulation, and underline a bandwidth of 290 MHz (4.9 %) associated with a gain of 6.4 dB at the frequency of 5.80 GHz.

Acknowledgments

This work was supported by the European Union through the European Regional Development Fund (ERDF) and by the Ministry of Higher Education and Research, Brittany Région, Côtes d'Armor Département and Saint Brieuc Armor Agglomération through the CPER Projects MATECOM and SOPHIE-STICC. This publication work was also supported by the Syndicat de Gestion du Pole Universitaire de Saint Brieuc (France). Authors greatly acknowledge J. Sol from IETR for DRA gain measurement.

References

[1] A. Petosa and A. Ittipiboon, Dielectric Resonator Antennas: A Historical Review and the Current State of the Art, Communications Research Centre Canada 3701 Carling Avenue, Ottawa, ON, K2H 8S2, Canada.

[2] R. K. Mongia and P. Bhartia, Dielectric Resonator Antennas-A Review and General Design Relations for Resonant Frequency and Bandwidth, Reviewed October 22, 1993; revised March I , 1994.

[3] S. A. Long, M. W. McAllister, and L. C. Shen, The resonant cylindrical dielectric cavity Antenna, IEEE Transactions on antennas and propagation, Vol. AP-31, MAY 1983.

[4] S. Sreekantan, Y. K. Ling, and Z. A. Ahmad M. F. Ain, M. B. Othman, and S. I. S. Hassan Simulation and experimental investigators on Rectangular, Circular and cylindrical dielectric resonator, Progress In Electromagnetics Research C, Vol. 7, 151–166, 2009**.**

[5] R. Kumari, K. Parmar and S. K. Behera, A Dual band Triangular shaped DRA Array for WLAN/WiMAX Applications. https://www.researchgate.net/publication/254048428

[6] K. Parmar, R. Kumari, S.K Behera. Half Cylindrical Dielectric Resonator Antenna for Dual Band Applications, April 2011.

[7] M.H. Neshati and Z. Wu. Theoretical and Experimental Investigation of Probe-fed Rectangular Dielectric Resonator Antennas. Electrical & Electronics Engineering Dept., UMIST, Manchester M60 1QD, UK.

[8] R. A. Kranenburg and S. A. Long. Microstrip transmission line excitation of dielectric resonator antennas. Electronics Letters, vol. 24, no. 18, pp. 1156-1157, 1 Sept. 1988, DOI: 10.1049/el:19880785.

[9] R.A. Kranenburg, S.A. Long, Microstrip transmission line excitation of dielectric resonator antennas, Electronics Letters 24 (1988) 1156-1157.

[10] A. A. Kishk, A. Ittipiboon, Y. M. M. Antar and M. Cuhaci, "Slot excitation of the dielectric disk radiator," in IEEE Transactions on Antennas and Propagation, vol. 43, no. 2, pp. 198-201, Feb. 1995, doi: 10.1109/8.366382.

[11] Aldo Petosa, Apisak Ittipiboon, and Michel Cuhaci, Dielectric Resonator Antenna Technology for Wireless Applications, Communications Research Centre, 3701 Carling Ave., P.O. Box 11490, Station H, Ottawa, ON, Canada, K2H 8S2

[12] Y. M. M. Antar, New directions in antenna research using dielectrics, Proceedings of the Twentieth National Radio Science Conference (NRSC'2003) (IEEE Cat. No.03EX665), Cairo, Egypt, 2003, pp. INV1-1, doi: 10.1109/NRSC.2003.157309.

[13] Yu-Ching Huang, Ming-Chung Wu, Tze-Hsuan Chang, Jean-Fu Kiang, Wei-Fang Su, Broadband DR Antenna made of high-Q ceramic, Journal of the European Ceramic Society, Volume 27, Issues 8–9, 2007, Pages 2841-2844, ISSN 0955-2219, https://doi.org/10.1016/j.jeurceramsoc.2006.11.058.

[14] R. Gangwar, S.P Singh, M. Choudhary, N.K Singh, D.Kumar, G.Rao, R. James, Microwave dielectric properties of $(Zn_{1-x}Mg_x)TiO_3$ (ZMT) ceramics for dielectric resonator antenna

application, Journal of Alloys and Compounds October 2011 509(42):10195–10202, DOI: 10.1016/j.jallcom.2011.08.028.

[15] S. Ballav, S.K Parui, Performance enhancement of dielectric resonator antenna by using cross-resonator based filtering feed-network, AEU - International Journal of Electronics and Communications, Volume 114, 2020, 152989, ISSN 1434-8411, https://doi.org/10.1016/j.aeue.2019.152989.

[16] S. Agrawal, R.D Gupta, M.S Parihar, P.N Kondekar, A wideband high gain dielectric resonator antenna for RF energy harvesting application, AEU - International Journal of Electronics and Communications, Volume 78, 2017, Pages 24-31, ISSN 1434-8411, https://doi.org/10.1016/j.aeue.2017.05.018.

[17] J. Plourde, D.Linn, H.Obryan Jr, J. John, $Ba_2Ti_9O_{20}$ as a Microwave Dielectric Resonator, Journal of the American Ceramic Society 58(9−10):418 – 420. October 2006.

[18] P. Mohanan, S. Mridula, B. Paul, N. Suma, P.V Bijumon, Sebastian, Mailadil. (2007). FDTD analysis of rectangular dielectric resonator antenna. Journal of the European Ceramic Society. 27. 2753-2757. DOI: 10.1016/j.jeurceramsoc.2006.11.053.

[19] F. Gheorghiu, C.E. Ciomaga, M. Simenas, M. Airimioaei, S. Qiao, S. Tascu, V. Kalendra, J. Banys, O.G. Avadanei, L. Mitoseriu, Preparation and functional characterization of magnetoelectric $Ba(Ti_{1-x}Fe_x)O_{3-x/2}$ ceramics. Application for a miniaturized resonator antenna, Ceramics International, Volume 44, Issue 17, 2018, Pages 20862-20870, ISSN 0272-8842, https://doi.org/10.1016/j.ceramint.2018.08.091.

[20] S. Parida, S.K. Rout, V. Subramanian, P.K. Barhai, N. Gupta, V.R. Gupta, Structural, microwave dielectric properties and dielectric resonator antenna studies of $Sr(Zr_xTi_{1-x})O_3$ ceramics, Journal of Alloys and Compounds, Volume 528, 2012, Pages 126-134, ISSN 0925-8388,

https://doi.org/10.1016/j.jallcom.2012.03.047.

[21] D.V.M. Paiva, M. A. S. Silva, R.G.M. de Oliveira, A.R Rodrigues, L.M.U.D Fechine, A.S.C Sombra, L.M.U.D Fechine. Magneto-dielectric composite based on $Y_3Fe_5O_{12}$ – $CaTiO_3$ for radio frequency and microwave applications. Journal of Alloys and Compounds (2018). 783. DOI: 10.1016/j.jallcom.2018.12.366.

[22] R.G.M. Oliveira, R.A. Silva, J.E.V. de Morais, G.S. Batista, M.A.S. Silva, J.C. Goes, H.D. de Andrade, I.S. Queiroz Júnior, C. Singh, A.S.B. Sombra, Effects of CaTiO3 addition on the microwave dielectric properties and antenna properties of BiVO4 ceramics, Composites Part B: Engineering Volume 175, 2019, 107122, ISSN 1359-8368, https://doi.org/10.1016/j.compositesb.2019.107122.

[23] Y. Hao, Q. Wang, X. Gao, S. Huang, K. Bi, Frequency tunable slot-coupled dielectric resonators antenna, Journal of Alloys and Compounds 702 (2017) 664-668.

[24] I- M. Reaney, D. Iddles, Microwave Dielectric Ceramics for Resonators and Filters in Mobile Phone Networks, Journal of the American Ceramic Society 89 (2006) 2063-2072.

https://doi.org/10.1111/j.1551-2916.2006.01025.x.

[25] S. Nanamatsu, M. Kimura, K. Doi, S. Matsushita, N. Yamada, Ferroelectrics, vol. 8, n° 1, pp. 511–513, Jan. 1974.

[26] F. Marlec, C. Le Paven, F. Cheviré, L. Le Gendre, R. Benzerga, B. Guiffard, T. Dufay, F. Tessier, B. Messaid, A. Sharaiha, Journal of the European Ceramic Society, vol. 38, n°6, pp.2526-2533, 2018.

[27] B.Filali, J.Rhazi, G.Ballivy, measuring dielectric properties of concrete by a wide coaxial probe with an open end. DOI - 10.1139/p06-056. Canadian Journal of Physics.

[28] C.L. Pournaropoulos et D.K. Misra. IEEE Trans. Instrum. Meas. 43, 111 (1994).

[29] B.W. Hakki, P.D. Coleman. A Dielectric Resonator Method of Measuring Inductive Capacities in the Millimeter Range. Transactions on microwave theory and techniques.

[30] J. Krupka, K. Derzakowskiz, B. Riddlex and J. Baker-Jarvis. A dielectric resonator for measurements of complex permittivity of low loss dielectric materials as a function of temperature. Jerzy Krupka et al 1998 Meas. Sci. Technol.9 1751.

[31] E.J Vanzura, R.G Geyer and M.D Janezic, The NIST60-millimeter diameter cylindrical cavity resonator, 1993, performance evaluation for permittivity measurements Natl Inst. Stand. Technol. Technical Note 1354.

[32] L. Huitema, T. Monediere, "Dielectric Materials for Compact Dielectric Resonator Antenna Applications," http://dx.doi.org/10.5772/50612.

[33] K.M Luk and K.W Leung, Dielectric Resonator Antennas. Electronic & Electrical Engineering Research Studies

[34] S. Keyrouz, D. Caratelli, Dielectric Resonator Antennas: Basic Concepts, Design Guidelines, and Recent Developments at Millimeter-Wave Frequencies, International Journal of Antennas and Propagation 2016 (2016) ID 6075680.

https://doi.org/10.1155/2016/6075680.

[35] J. D. Kraus, Antennas for all applications, Second Edition, McGraw-Hill Company, 1997.

[36] L. Zhang, W.L. Zhong, C.L. Wang, Y.P. Peng, and Y.G. Wang, Size dependence of dielectric properties and structural metastability in ferroelectrics. Eur. Phys. J. B-Condens. Matter Complex Syst., vol. 11, no. 4, pp. 565–573, 1999.

[37] L. Zhang, W.L. Zhong, C.L. Wang, P.L. Zhang, and Y.G. Wang, Finite-size effects in ferroelectric solid solution. J. Phys. Appl. Phys., vol. 32, no. 5, p. 546, 1999.

[38] A. Hushur, G. Shabbir, J.H. Ko, S. Kojima, The phase transitions of ferroelectric $Sr_2Ta_2O_7$ crystals by MDSC, Brillouin and dielectric spectroscopy, J. Phys, D: Apply. Phys. 37 (2004) 1127-1131.

[39] J. Song, Ferroelectric thin films for high density non-volatile memories, Doctoral Dissertation Virginia Polytechnic Institute and State University (1998).

[40] R. A. Burberry, VHF and UHF antennas. London: P. Peregrinus on behalf of the Institution of Electrical Engineers, 1992.

[41] D. Kajfez, A. W. Glisson and J. James, "Computed Modal Field Distributions for Isolated Dielectric Resonators," in IEEE Transactions on Microwave Theory and Techniques, vol. 32, no. 12, pp. 1609-1616, Dec. 1984, doi: 10.1109/TMTT.1984.1132900.

[42] K. W. Leung, K. Y. Chow, K. M. Luk, and E. K. N. Yung, Low-Profile Circular Disk DR Antenna of Very High Permittivity Excited by a Microstrip line. IEEE Electronics Letters, 33, 12, June 1997, pp. 1004 - 1005.

[43] Z. Wang, C. C. Chi au, X. Chen, B. S. Collins, and S. P. Kingsley, A Miniature Broadband Dielectric Resonator Antenna (DRA) Operating at 2.4 GHz. International Workshop, Antenna Technology: Small Antennas and Novel Metamaterials, New York, NY, March 2006, pp. 104-107.

[44] F.R Hsiao, C. Wang, K.L Wong and T.W Chiou, Broadband very-high-permittivity dielectric resonator antenna for WLAN application. IEEE Antennas and Propagation Society International Symposium (IEEE Cat. No.02CH37313), San Antonio, TX, USA, 2002, pp. 490-493 vol.4.

[45] Zhen Peng, Hong Wang, Xi Yao, Dielectric resonator antennas using high permittivity ceramics, Ceramics International, Volume 30, Issue 7, 2004, Pages 1211-1214, ISSN 0272-8842,

https://doi.org/10.1016/j.ceramint.2003.12.079.

[46] M. T. Sebastian, R. Ubic, H. Jantunen, Low-loss dielectric ceramic materials and their properties, International Materials Reviews, Pages 392-412,

https://doi.org/10.1179/1743280415Y.0000000007

Figure 1. Schematic representation of the dielectric resonator antenna geometry (generated by the CST software).

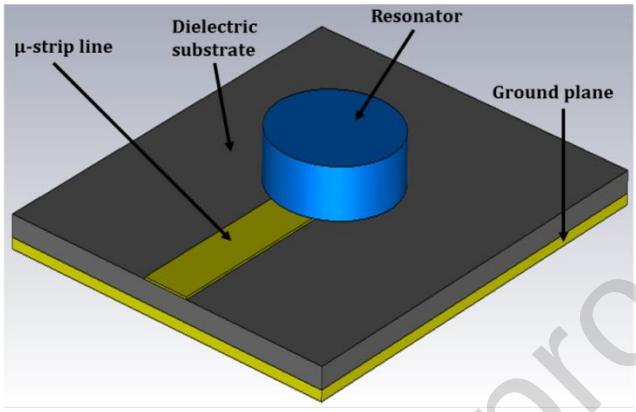

Figure 2. Evolution as a function of the composition (x) of the relative variation of the lattice parameters (a, b, c) and of the volume of the orthorhombic cell of the $(Sr_2Ta_2O_7)_{100-x}(La_2Ti_2O_7)_x$ synthesized powders. The uncertainty on the values is shorter than the size of the markers.

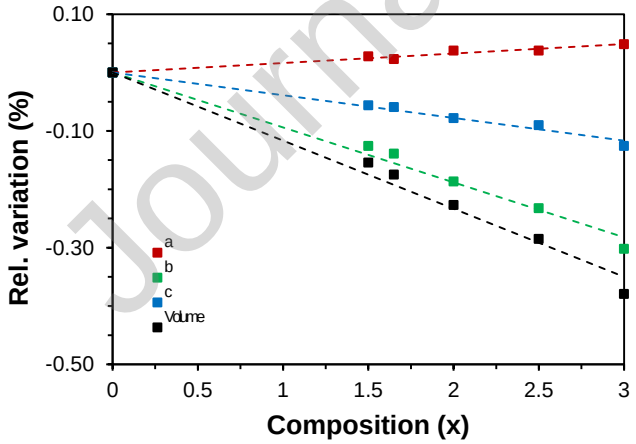

Figure 3. Evolution as a function of the composition (x) of the grain size of the $(Sr_2Ta2O7)_{100-x}(La_2Ti_2O_7)_x$ ceramics sintered at 1500°C during 2h under air (except the composition x = 0 sintered at 1400°C).

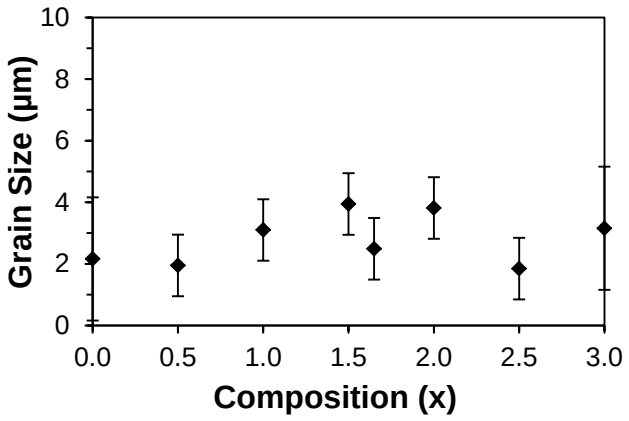

Figure 4. Evolution, at 10 kHz and RT, of the permittivity (ε') and dielectric losses (tanδ) as a function of the composition (x) of $(Sr_2Ta_2O_7)_{100-x}(La_2Ti_2O_7)_x$ ceramics. MIM measurements with a LCR meter.

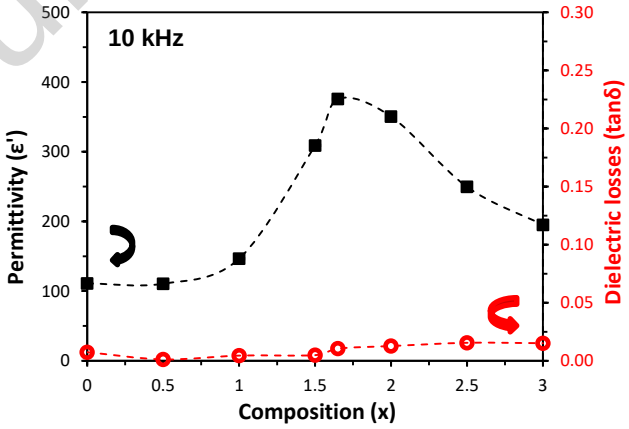

Figure 5. Evolution, at 2 MHz and RT, of the permittivity (ε') and dielectric losses (tanδ) as a function of the composition (x) of $(Sr_2Ta_2O_7)_{100-x}(La_2Ti_2O_7)_x$ ceramics. MIM measurements with a vector network analyzer.

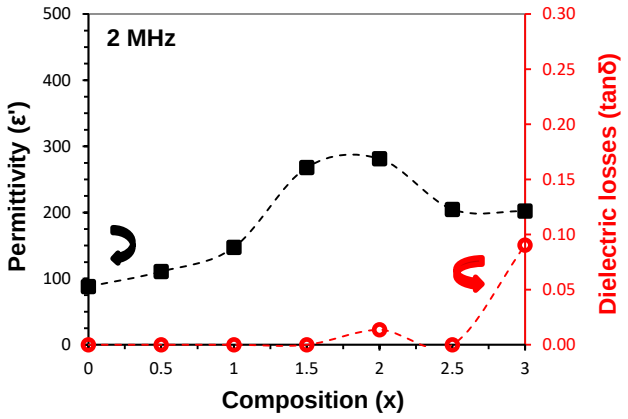

Figure 6. Evolution, at 2 GHz and RT, of the permittivity (ε') and dielectric losses (tanδ) as a function of the composition (x) of $(Sr_2Ta_2O_7)_{100-x}(La_2Ti_2O_7)_x$ ceramics. Measurements with a dielectric coaxial probe.

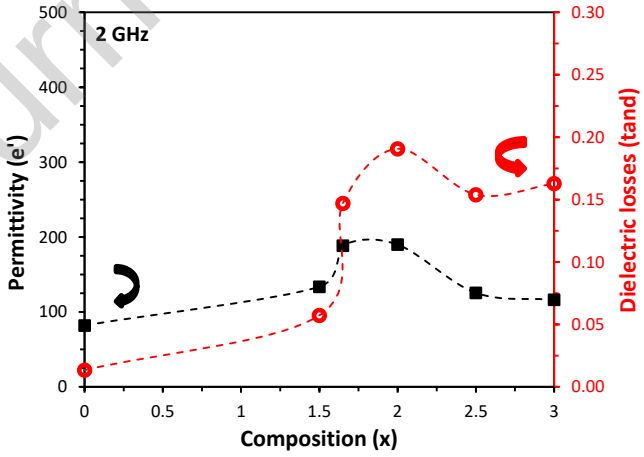

Figure 7. Evolution, around 2 GHz and at RT, of the permittivity (ε') and dielectric losses (tanδ) as a function of the composition x of $(Sr_2Ta_2O_7)_{100-x}(La_2Ti_2O_7)_x$ ceramics. Measurements with a dielectric resonator cavity.

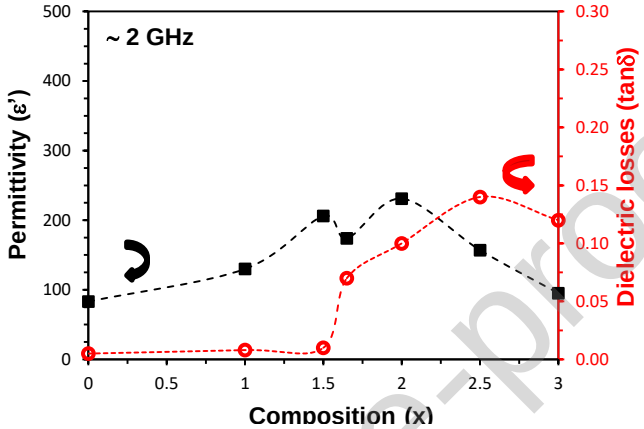

Figure 8. (a) Geometry of the simulated dielectric resonator antenna using CST studio and (b) realized prototype based on a STLTO ceramic with x = 0 .

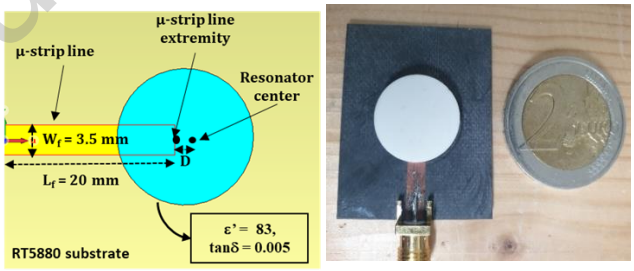

(a) **(b)**

Figure 9. *S_{11} reflection parameter for the simulated (solid line) and for the measured (dotted line) structure of the dielectric resonator antenna based on a STLTO ceramic with x = 0.*

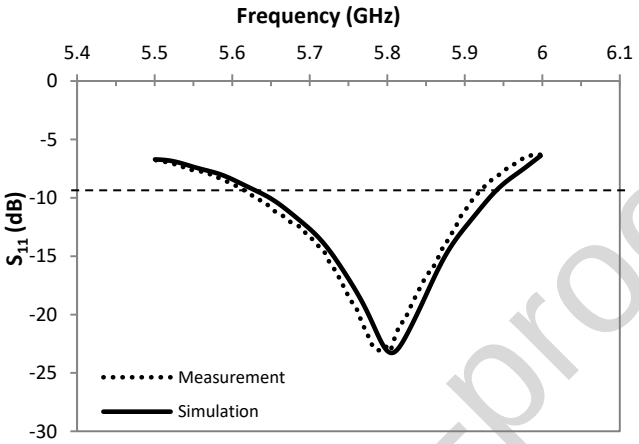

Figure 10. Simulation of the electric and magnetic field distributions made by CST inside the cylindrical DRA: (a) top view : E-field (b) top view : H-field (c) side view : E-field (d) side view : H-field. In black are drawn, in each case, the theoretical distribution of the $HEM_{11\delta}$ mode [42-43].

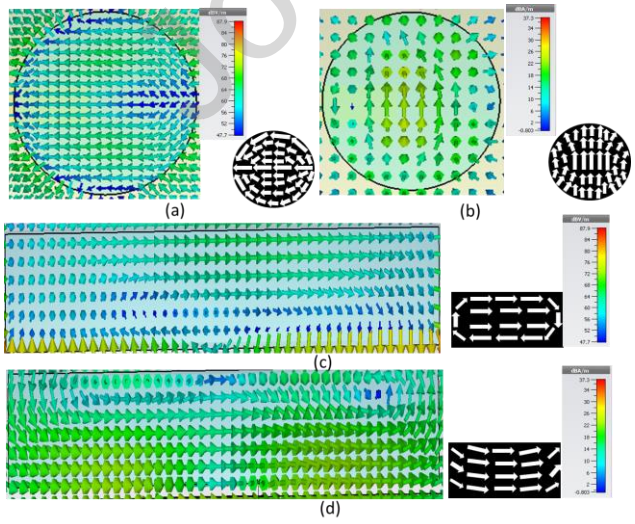

Figure 11. *Simulated (solid line) and measured (dotted line) radiation patterns at 5.8 GHz in the E plane for (a) ϕ = 0 ° and in the H plane (b) for ϕ = 90 ° of the dielectric resonator antenna based on a STLTO ceramic with x = 0 (co-polar in black and cross polar in red).*

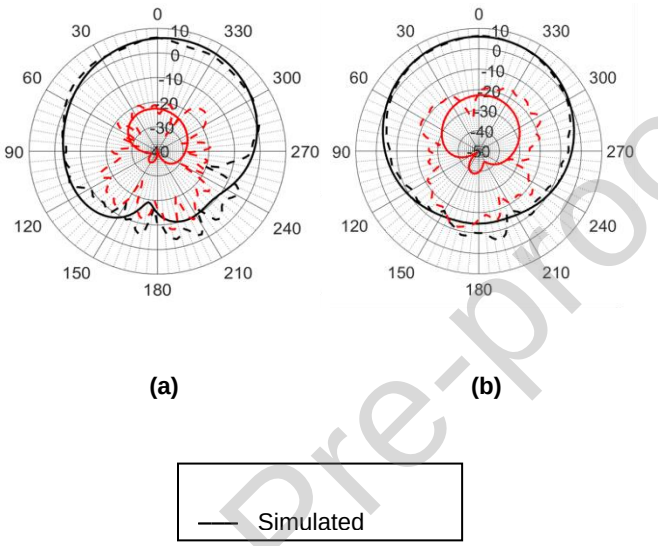

Table 1. *Characteristics of the cavity and STLTO ceramic samples for the QWED cavity measurement.*

x	F_R (GHz)	Q	ε'	tanδ
0	3.32	180	83	5×10^{-3}
1.0	2.68	113	130	8×10^{-3}
1.5	2.16	75	206	1×10^{-2}
1.65	2.24	13	174	7×10^{-2}

2.0	1.98	10	230	1.0×10^{-1}
2.5	2.26	7	157	1.4×10^{-1}
3.0	3.34	8	95	1.2×10^{-1}

Table 2. *Reported characteristics of DRA's with dielectric materials having permittivities in the range of those of the STLTO material used in the present study.*

Form	**Radius or dimensions (mm)**	**Height (mm)**	**Resonance frequency (GHz)**	**Permittivity ε'**	**Excitation type**	**Bandwidth BW (%)**	**Gain (dB)**	**Ref**
Cylindrical	12.5	2	4.18	82	Microstrip	3.6	5	[42]
Cylindrical (complex form)	15 x 6	5	2.40	90	Microstrip	5.0	-	[43]
Rectangular	28 x 28	4.6	5.2	90	Microstrip	4.8	4.1	[44]
Cylindrical	5.2	9.12	2.6	96.7	Coaxial probe	1.5	-	[45]
Cylindrical	7.1	6.57	3.76	82	Coaxial probe	1.2	-	[20]
Cylindrical	7.95	2.32	5.8	83	Microstrip	5.0	6.4	**Present results**